HHS Public Access

Author manuscript

Cell Stem Cells Regen Med. Author manuscript; available in PMC 2016 December 28.

Published in final edited form as:

Cell Stem Cells Regen Med. 2016 November ; 2(2): .

Temporary, Systemic Inhibition of the WNT/β-Catenin Pathway promotes Regenerative Cardiac Repair following Myocardial Infarct

Dikshya Bastakoty[1], **Sarika Saraswati**[1,†], **Piyush Joshi**[2], **James Atkinson**[1,3], **Igor Feoktistov**[4], **Jun Liu**[5], **Jennifer L Harris**[5], and **Pampee P Young**[1,3,6,*]

[1]Department of Pathology, Microbiology, and Immunology, Vanderbilt University Medical Center, Nashville, Tennessee, USA

[2]Interdisciplinary Graduate Program, Vanderbilt University Medical Center, Nashville, Tennessee, USA

[3]Department of Veterans Affairs Medical Center, Nashville, Tennessee, USA

[4]Division of Cardiovascular Medicine, Vanderbilt University Medical Center, Nashville, Tennessee, USA

[5]Genomics Institute of Novartis Research Foundation, San Diego, California, USA

[6]Department of Internal Medicine, Vanderbilt University Medical Center, Nashville, Tennessee, USA

Abstract

Aims—The WNT/β-catenin pathway is temporarily activated in the heart following myocardial infarction (MI). Despite data from genetic models indicating both positive and negative roles for the WNT pathway depending on the model used, the effect of therapeutic inhibition of WNT pathway on post-injury outcome and the cellular mediators involved are not completely understood. Using a newly available, small molecule, GNF-6231, which averts WNT pathway activation by blocking secretion of all WNT ligands, we sought to investigate whether therapeutic inhibition of the WNT pathway temporarily after infarct can mitigate post injury cardiac dysfunction and fibrosis and the cellular mechanisms responsible for the effects.

Methods and Results—Pharmacologic inhibition of the WNT pathway by post-MI intravenous injection of GNF-6231 in C57Bl/6 mice significantly reduced the decline in cardiac function

[*]**Corresponding author:** Pampee P. Young, Department of Pathology, Vanderbilt University Medical Center, 1161 21st Ave. South C2217A MCN, Nashville, TN 37232, USA, Tel: (615) 936-1098; Fax: (615) 343-702; pampee.young@vanderbilt.edu.
[†]Current affiliation: Department of Veterans Affairs Medical Center, Nashville, TN, USA

Author Contributions

DB and PPY designed the study. DB, SS, PJ, JA, JL and JLH performed experiments and collected data from experiments. DB, SS, JL and PPY analyzed the data, IF, JL and JLH provided reagents and helped in data analysis and provided conceptual advice. DB, JL, JLH and PPY wrote the manuscript.

Conflicts of Interests

JL and JLH are employees of the Novartis Research Foundation. PPY is listed as inventor for a WNT inhibitory topical therapeutic.

(Fractional Shortening at day 30: 38.71 ± 4.13% in GNF-6231 treated vs. 34.89 ± 4.86% in vehicle-treated), prevented adverse cardiac remodeling, and reduced infarct size (9.07 ± 3.98% vs. 17.18 ± 4.97%). WNT inhibition augmented proliferation of interstitial cells, particularly in the distal myocardium, inhibited apoptosis of cardiomyocytes, and reduced myofibroblast proliferation in the peri-infarct region. *In vitro* studies showed that WNT inhibition increased proliferation of $Sca1^+$ cardiac progenitors, improved survival of cardiomyocytes, and inhibited collagen I synthesis by cardiac myofibroblasts.

Conclusion—Systemic, temporary pharmacologic inhibition of the WNT pathway using an orally bioavailable drug immediately following MI resulted in improved function, reduced adverse remodeling and reduced infarct size in mice. Therapeutic WNT inhibition affected multiple aspects of infarct repair: it promoted proliferation of cardiac progenitors and other interstitial cells, inhibited myofibroblast proliferation, improved cardiomyocyte survival, and reduced collagen I gene expression by myofibroblasts. Our data point to a promising role for WNT inhibitory therapeutics as a new class of drugs to drive post-MI repair and prevent heart failure.

Keywords

WNT/β-Catenin Pathway; Regenerative cardiac repair; Myocardial infarct

Introduction

Cardiovascular disease is the leading cause of death in the United States, and coronary heart disease, which leads to ischemic myocardial injury is the most common cardiovascular disease with a toll of 370,000 deaths each year in the US [1]. Cardiomyocyte apoptosis and fibrosis initiated by an infarct result in continuing adverse remodeling of the myocardium, which leads to eventual heart failure [2,3]. Current therapies for MI focus mostly on disease management and prevention of MI recurrence. Hence, there is a need to develop effective therapeutics that addresses the core pathophysiology, particularly the ongoing cardiomyocyte death and fibrosis that occur in the aftermath of an infarct.

The WNT/β-catenin pathway is activated in various cardiac cells in response to ischemic injury [4,5], and has been studied by many groups in the context of myocardial infarct repair. In genetic models of WNT pathway modulation through β-catenin stabilization or depletion in cardiomyocytes, WNT activation leads to adverse remodeling after ischemic injury, whereas WNT inhibition improves function [6,7]. Studies using overexpression or exogenous administration of secreted WNT inhibitors (secreted Frizzled-Related Protein 1 and 2; sFRP1, and sFRP2 [8,9]) have shown that WNT inhibition stimulates recovery of cardiac function and reduces scarring after MI, although the cellular mechanisms proposed by these studies have been different. Distinct and incomplete blocking of ligand-dependent vs. independent WNT signaling [10], or in the case of pyrvinium [11,12], incomplete therapy due to toxicity and effects on other signaling pathways, may account for the differences in cellular effects of WNT inhibitory therapeutics observed in these studies.

Moreover, there are conflicting reports suggesting that WNT activation can also enhance post-MI cardiac repair. Paik et al. [13] showed that gain-of-function of a canonical WNT ligand, WNT 10b, in cardiomyocytes can orchestrate recovery by augmenting

neovascularization. Interruption of WNT 1/β-catenin signals specifically in the epicardium through β-catenin deletion was reported to impede adaptive pro-fibrotic response [14,15], whereas post-infarct injection of adenoviral vector with constitutively active β-catenin reduced infarct size by boosting cardiomyocyte survival, and granulation tissue formation by myofibroblasts [16]. Some of the discrepant observations may be explained by ligand [15] and cell-type dependent [16] effects of WNT signaling on healing. Moreover, the genetic models that use cell-specific promoters to modulate WNT signaling have caveats, such as incomplete targeting of the microenvironment, inability to transiently inhibit the signal, and unintended physiological effects on the cell types targeted (for example, complete β-catenin mutation in epicardial cells [14] may lead to deficiencies in the developing heart as reported in previous studies [17] complicating the investigation of its effect on the infarcted heart).

We hypothesized that short term WNT inhibition with a pharmacologic agent that comprehensively targets all WNT ligand-dependent signaling improves cardiac recovery following MI in a mouse model of permanent ligation of the left ventricle descending coronary artery by affecting multiple cardiac cells to mediate repair. The paucity of safe and effective WNT inhibitors suited for clinical use has delayed efforts to assess therapeutic WNT pathway inhibition in cardiac injury [18,19]. Recently, with the new class of WNT ligand secretion inhibitors, that act on the membrane-bound O-acyltransferase, Porcupine [20], we are able to investigate the potential of systemic WNT inhibition for post-MI cardiac injury repair. The enzyme Porcupine palmitoylates WNT ligands—a modification is essential for the secretion and receptor binding of WNT proteins [21]. It has been shown that Porcupine activity is specific to WNT ligands and does not affect other similarly lipid modified signaling proteins such as Hedgehog [22], hence making it a suitable candidate for WNT pathway targeting. For our studies, we used GNF-6231, a Porcupine inhibitor synthesized by the Genomics Institute of the Novartis Research Foundation. An analog of the compound, LGK974 [21], has already advanced to clinical studies for WNT-driven cancers [23]. Here we report that short-term pharmacologic WNT inhibition following experimental MI augments cardiac repair, characterized by improvement in functional and remodeling parameters, and reduction in collagenous scar. Our data suggest that this occurs through effects on multiple facets of cardiac pathology including, proliferative response in interstitial (possibly, progenitor) cells in the heart, through reduction in cardiomyocyte apoptosis, and through mitigation of myofibroblast proliferation and collagen synthesis.

Materials and Methods

Antibodies

The following antibodies were used: β-catenin (1:200; BD Pharmingen, 610153); β-galactosidase (1:100; AbCam, Ab616); Alpha Smooth Muscle Actin (α-SMA) (1:1000; Sigma A2547); Ki67 (1:400; AbCam, Ab15580); phospho-Histone-H3 (1:200; Millipore, 06-570); cTnI (1:1000; AbCam, Ab6556); Alpha Sarcomeric Actin (1:200; Sigma, A2172); GATA4 (1:200; Santa Cruz, SC25310); Periostin (1:100; Santa Cruz, SC67233); PCNA (1:100; Santa Cruz Biotech, SC-56); FSP1 (1:100; Millipore, 07-2274); Vimentin (1:200; Sigma, V2258); vWF (1:200; Takara, M116).

WNT modulators

The small molecule Porcupine inhibitor GNF-6231 was a generous gift from the Genomic Institute of the Novartis Research Foundation. Small molecule WNT inhibitor (CK1α activator) VU-WS113 (C-113) was a generous gift from Dr. Ethan Lee, Department of Cell and Developmental Biology, Vanderbilt University [24]. Recombinant mouse WNT3A was purchased from AbCam (ab81484) or from the Vanderbilt Antibody and Protein Resource (VAPR). For *in vitro* studies, GNF-6231 in DMSO as vehicle was used at a concentration of 100 nM; C-113 (vehicle: DMSO) was used at 1 μM; and recombinant mouse WNT3A (vehicle: 01% BSA in PBS) was used at a concentration of 50 ng/mL after testing a range of concentrations between 25 ng/ml–100 ng/ml and demonstrating similar proliferative response (data not shown).

Animals

All procedures were carried out in accordance with Vanderbilt Institutional Animal Care and Use Committee (IACUC), and NIH guidelines. C57Bl/6J mice were purchased from the Jackson Laboratory (Bar Harbor, ME) and maintained by PPY. TOPGAL [5] mice were a generous gift from Dr. Antonis Hatzopoulos (Department of Cell and Developmental Biology, Vanderbilt University).

Cell lines

$Sca1^{+}CD31^{-}CD45^{-}$ cells were isolated as previously described [25]. Briefly, H-$2K^{b}$-tsA58 transgenic mice in C57Bl/6 background expressing temperature sensitive thermolabile simian virus (SV40) large tumor (T) antigen under the ubiquitous mosue major histocompatibility complex (H-$2K^{b}$) promoter—age 6- to 8-weeks—were euthanized using overdose of Isoflurane followed by cervical dislocation. Hearts from five mice were dissected to isolate ventricular tissue, which was then minced and incubated with 10 ml of digestion solution (10 mg/ml collagenase II, 2.5 U/ml dispase II, 1 μg/ml, DNase I, and 2.5 mM $CaCl_2$) for 20 min at 37°C. The non-myocytes were collected using Percoll gradient. A filtered myocyte-free single-cell suspension in PBS containing 0.5% BSA and 2 mM EDTA (PBS/BSA/EDTA) was treated with mouse BD Fc Block (clone 2.4G; BD Biosciences, San Jose, CA), and immune cells were magnetically removed with CD45 microbeads (Miltenyi Biotec Inc., Auburn, CA). After incubation with phycoerythrin (PE)-conjugated CD31 (clone 390; eBioscience, San Diego, CA) and fluorescein isothiocyanate (FITC)-conjugated Sca1 (clone E13-161.7; BD Biosciences) antibodies, CD31 positive cells were removed with anti-PE microbeads (Miltenyi Biotec). $Sca1^{+}CD31^{-}$ cells were magnetically isolated with anti-FITC microbeads (Miltenyi Biotec). Isolated conditionally immortalized $Sca\text{-}1^{+}CD31^{-}CD45^{-}$ cells were plated at a density of 10^{4} cell/cm^{2} and cultured on 1% gelatin-coated tissue culture dishes in DMEM supplemented with 10% FBS, 1% Penicillin/Streptomycin, and 2 mM glutamine and 10 ng/ml IFN-γ under a humidified atmosphere of air/CO_2 (19:1) at 33°C. Six days before experiments, cells were replated and cultured in the absence of IFN-γ at 37°C.

HL1 cell line, derived from mouse atrial cardiomyocytes was a kind gift from Dr. William C. Claycomb (Louisiana State University Medical Center, New Orleans, LA). These cells were cultured on gelatin/fibronectin (25 μg fibronectin in 2 ml of 0.02% gelatin in water)- coated

plates (fibronectin and gelatin from Sigma-Aldrich). The HL1 cell line was maintained at 37°C in Claycomb medium (SAFC Biosciences, Lenexa, KS) supplemented with 10% fetal bovine serum (SAFC Biosciences), 100 μM norepinephrine (Sigma) in 30 mM ascorbic acid (Sigma), 2 mM L-Glutamine (Sigma), penicillin, and streptomycin (Life Technologies, Grand Island, NY).

iCell Plus Cardiomyocytes, which are primarily ventricular cardiomyocytes derived from human induced pluripotent stem (iPS) cells, were purchased from Cellular Dynamics International and maintained in 0.1% gelatin coated plastic plates in manufacturer's proprietary maintenance medium.

Primary mouse cardiac fibroblasts were isolated from the hearts of C57Bl/6 mice that were at least 12 weeks old following a previously described protocol [26]. Briefly, mice were euthanized by overdose of isoflurane followed by cervical dislocation. Heart tissue was minced and placed into Kreba-Henseleit (Sigma; K3753a) buffer with 2.9 mM $CaCl_2$ and 24 mM $NaHCO_3$ containing a cocktail of 0.25 mg/mL Liberase Blendzyme 3 (Roche Applied Science), 20 U/mL DNase I (Sigma Aldrich), 10 mmol/L HEPES (Invitrogen) and 0.1% sodium azide in HBSS, and shaken at 37°C for 20 min. Cells collected after digestion were passed through 40 μm nylon mesh and centrifuged (15 min, 200 g, 4°C). Finally, cells were reconstituted with DMEM-F12 medium containing 10% FBS and 1% Penicillin/Streptomycin and seeded onto plastic plates (Corning) for separation of fibroblasts by selective adhesion for 4 hours at 37°C. Cells were maintained in culture medium composed of high glucose (4.5 g/L) DMEM with 10% FBS and 1% Penicillin/Streptomycin under a humidified atmosphere of air/CO_2 (19:1) at 37°C.

Proliferation assay

Cell proliferation was assessed by 5-bromo-2′-deoxyuridine (BrdU) cell proliferation assay (Calbiochem, Gibbstown, NJ). Briefly, CPCs, HL-1 cells, or primary fibroblasts were seeded on 96-well plates (gelatin/fibronectin-coated for HL-1 cells), with recombinant WNT3A where indicated. Following attachment onto plates, WNT modulators were added and cultured for 24 hours. BrdU incorporation was assessed by enzyme-linked immunosorbent assay (ELISA) and read at a dual wavelength of 450/595 nm using the SOFTMax Version 2.35 software (Molecular Devices, LLC, Sunnyvale, CA) following manufacturer's recommendations.

Cell viability assay

HL-1 cardiomyocytes were serum starved overnight in 2% FBS, and seeded onto (gelatin/fibronectin-coated for HL-1) 96-well plate at a density of 10^4 cells/well. Following attachment of cells over 24 hours, WNT modulators (50 ng/mL recombinant mouse WNT3A with or without 1 μM C-113) were added and the cells incubated for 48 hours. Cell viability was assessed by incubating with 0.5 mg/mL of 3-[4,5-dimethylthiazol-2-yl] 2,5,-diphenyltetrazolium bromide (MTT) (Sigma) in PBS for 4 hours at 37°C, and MTT reduction into formazan by viable cells was measured. Formazan crystals were dissolved in 75 μL/well DMSO 10 minutes at 37°C. Photometric measurement was carried out at 540 nm. Percentage viability was calculated by as follows: %Cell

survival=($OD_{Control}$−OD_{Sample}) × 100%/$OD_{Control}$. Untreated cells were used as control. Results represent three independent experiments, each performed in triplicate.

Surgical LAD ligation (myocardial infarction) model, drug treatment, echocardiography and infarct size calculations

Male C57Bl6J mice (at least 3 months of age) were anesthetized under sodium pentothal (50 mg/kg) and endotracheal intubation was performed under direct laryngoscopy. Mice were ventilated with a small animal respirator (tidal volume=1.0 ml, rate=110 breaths/min). With the use of a surgical microscope, a left thoracotomy was performed. The fourth intercostal space was entered using scissors and blunt dissection. A 7-0 silk suture was placed through the myocardium into anterolateral LV wall and the left anterior descending artery was ligated. The heart was monitored with continuous EKG throughout the procedure to ensure successful infarction. The chest was closed in layers with 6-0 silk (6-0 nylon to close the skin) and the animal was gradually weaned from the respirator to avoid complicating pneumothorax. Intraperitoneal administration of 0.1 mg/kg buprenorphine immediately following surgery and every 8–12 hours for 72 hours post-surgery was used as analgesic. Animals were monitored closely for signs of distress and weight loss throughout the study period. Severe respiratory distress, lack of ambulation, or severe weight loss (>20–30% of body weight) was considered reasons for euthanizing the animal. Following study completion, or upon distress, animals were euthanized by overdose of isoflurane followed by cervical dislocation.

Starting from within 6 hours after surgery through day 6 post-infarct, mice were treated every 24 hours with intravenous (tail-vein) injection of 5 mg/kg (100 μL volume) GNF-6231 or vehicle (3% D-α-tocopheryl polyethylene glycol succinate or Vitamin E in 20% Polyethylene glycol).

For cardiac recovery study, cardiac dimensions were obtained from 2-D guided M-mode images (100 frames/sec) and were read blinded using short axis and a parasternal long-axis views. All measurements were done on unsedated mice at day 7 and day 30 post-MI. Measurements were averaged over 3 consecutive beats from the LV posterior wall (LVPW) the interventricular septum (IVS) and LV internal diameter (LVID). After day 30 echocardiography, hearts were excised, immersion-fixed in and paraffin-embedded to obtain serial sections in order to measure the infarct size (% area of tissue stained blue for collagen in H&E stained sections) in a blinded manner.

Separately, for longitudinal studies, hearts were excised at day 3, 7, and 15 days post MI, and processed to obtain paraffin sections for immunostaining studies.

Histology and morphometry

Hearts were fixed in 10% buffered formalin for 24 hours, embedded in paraffin and sectioned into 5 microns-thick transverse sections. H&E and Masson’s trichrome staining was performed by the Vanderbilt Translational Pathology Shared Resource. Olympus DP71 microscope camera (Olympus America, Center Valley, PA) was used for imaging H&E and Masson’s trichrome stained sections.

For immunofluorescence staining, slides were deparaffinized and hydrated through xylene and ethanol steps. Heat-mediated antigen retrieval was performed by boiling in citrate buffer (pH 6). Cells seeded onto coverslips were fixed for 1 hour at room temperature in 1% paraformaldehyde, permeabilized with 0.1% Triton-X in 0.1% sodium citrate for 2 min on ice, and washed several times with PBS. Following blocking with 10% goat serum in 1% BSA solution for 1 hour at room temperature, sections were incubated with primary antibody at 4°C overnight, and Alexa Fluor 488 or Cy3 conjugated secondary antibodies at room temperature for 1 hour. The slides were then counterstained with Hoechst 33342 (H21492 Invitrogen, Carlsbad, CA) and mounted with Slowfade Gold (S36936 Life Technologies, Grand Island, NY). For TUNEL staining, a 1:10 mix of enzyme:label diluted 5 fold with TUNEL dilution buffer (*In Situ* Cell Death Detection Kit TMR Red, Roche 12 156 792 910) was added to samples along with the secondary antibody and incubated for 60 minutes at 37°C. Samples were then counter stained with Hoeschst and mounted. Images were taken at 10×, 20× or 40× magnification using Axio Imager2 microscope (Carl Zeiss, Thornwood, NY) and CoolSNAP HQ CCD camera (Photometrics, AZ), and quantified using ImageJ. For confocal microscopy, LSM510 (Zeiss) microscope was used to capture 1 μm optical slices. All images are presented with scale bars that equal 50 μm.

PK/PD study

Single dose PK/PD profile of GNF-6231 was investigated in C57Bl/6 mice following a 5 mg/kg intravenous bolus injection following guidance from manufacturer. The drug was dissolved in 20% Poly Ethylene Glycol (PEG) 300 with 3% D-α-Tocopherol polyethylene glycol 100 succinate (ETPGS) in H_2O. Briefly, GNF-6231 was homogenized using QIAGEN bead homogenizer for at least 10 minutes in the presence of 25% of the final volume of the vehicle to be used to form slurry. Another 25% of vehicle was added and bath sonicated on high for 10 minutes. The remaining volume of vehicle was added and vortexed. An additional 10 minute bath sonication was performed. Further, probe sonication was performed at 50% amplitude for 3× 30 seconds on ice bath. The reconstituted drug was filtered with a 0.45 μm syringe filter. Vehicle alone underwent similar preparation in the absence of GNF-6231. At specific time points following intravenous administration, blood was collected from the saphenous vein. Plasma concentrations of GNF-6231 were quantified by LC/MC/MS analysis. Briefly, aliquots of plasma samples were added to the internal standard and acetonitrile/methanol (3/1), samples were vortexed and centrifuged at 4,000 rpm for 5 minutes at 4°C to precipitate the plasma proteins. Supernatant was transferred to a clean 96-well plate, and diluted with distilled water. The extracted samples were injected (10 μL) onto a Zorbax SB-C8 analytical column (2.1 × 30 mm, 3.5 μm).

Agilent Technologies Inc., Palo Alto, CA, USA). Mobile phases consisted of 0.05% formic acid in water (solvent A) and 0.05% formic acid in acetonitrile (solvent B), and a gradient elution method at a flow rate of 700 μL/min was used for compound elution and separation. Mass spectral analyses were carried out using atmospheric pressure chemical ionization (APCI) in the positive ion mode, with multiple reaction monitoring (MRM) of GNF-6231 (449.2>221.0). The lower limit of quantitation (LLOQ) in plasma was 1.0 ng/mL. Pharmacokinetic parameters were calculated by non-compartmental regression analysis using an in house fitting program.

PD study was performed as described previously [21]. Briefly, livers were collected from mice at specific time points after GNF-6231 or vehicle injection following euthanasia with isoflurane overdose and cervical dislocation. Total RNA was isolated using the Qiagen RNeasy kit; TaqMan analyses were performed using *Axin2* and *Gapdh* probes (Applied Biosystems) according to the manufacturer's instructions. mRNA expression levels for the target gene, *Axin2*, was normalized to Gapdh mRNA levels and data were analyzed using SDS 2.0 software (Applied Biosystems) to calculate relative RNA quantities.

RNA isolation and qRT-PCR

RNA was isolated from cells were using Trizol Reagent (Invitrogen, 15596026) following manufacturer's protocol. First strand DNA synthesis was performed with 1 μg RNA using iScript cDNA synthesis kit (Bio-Rad 170-8890). Quantitative real-time PCR was performed in triplicate for each sample with iCycler (BioRad) and fluorescence detection (SsoFast EvaGreen; 172-5200; BioRad). Each reaction was normalized against 18S. Primer sequences are provided in supplementary Table S1.

Statistical analysis

The statistical significance between experimental and control groups were determined by One-way ANOVA with Bonferroni correction for multiple comparisons when multiple groups were compared. The D'Augustino and Pearson omnibus or the Shapiro-Wilk tests were used to determine whether the data sets were normally distributed. For data sets that were not normally distributed or had $N<7$, the Kruskal-Wallis H-test was used instead of One-way ANOVA. For comparison between two groups of data, unpaired t-test was used for normally distributed datasets, and Mann-Whitney test was used for data that were not normally distributed. GraphPad Prism (San Diego, CA) software was used for all statistical analyses. $P<0.05$ was considered statistically significant in two-tailed hypothesis tests.

Results

Porcupine inhibitor GNF-6231 downregulates WNT target gene expression, is bioavailable *in vivo*, and is well-tolerated by WNT-dependent tissues

In order to investigate the physiological and cellular effects of WNT inhibition on post-MI cardiac regeneration, we utilized GNF-6231, a small molecule inhibitor of the acyltransferase, Porcupine. Porcupine is the enzyme responsible for the post-translational palmitoylation of WNT proteins that is required for both WNT secretion as well as binding of WNTs to their receptors [21] (Figure 1A). An analog of the compound is currently in Phase I clinical trials as WNT inhibitory therapeutics for cancer [23]. GNF-6231 inhibits Porcupine enzymatic activity with a cellular IC50 of 0.8 nM, and does not show cytotoxicity up to 20 μM [27]. In *Wnt3a* overexpressing cardiac cells, it potently inhibited WNT pathway activation as indicated by *Axin2* mRNA levels (Figure 1B). *In vivo*, the pharmacokinetic (PK) and pharmacodynamic (PD) relationship of GNF- 6231 was investigated following a single 5 mg/kg intravenous administration of GNF-6231 or vehicle to C57BL/6J mice. GNF-6231 showed high plasma levels, and free plasma concentrations (mouse plasma protein binding of GNF-6231 is 88%) above its *in vitro* Porcupine IC50 for at least 12 h. Plasma half-life of GNF-6231 was estimated to be 2.3 hours (Figure 1C). The expression of

the WNT target gene *Axin2* was measured in liver tissues. Although reduction in *Axin2* gene expression in the liver by GNF-6231 treatment started by 3 hours after a single intravenous injection, a statistically significant reduction occurred at 7 hours post-treatment. At 24 hours, there was a 37% reduction in *Axin2* expression compared to vehicle, indicating successful WNT inhibition at that time point (Figure 1D). Since GNF-6231 inhibits the enzymatic activity of Porcupine, impeding WNT secretion, an expected time delay was observed between peak GNF-6231 plasma concentration (5 min) and the PD response as measured by *Axin2* inhibition (Figure 1D).

Since the canonical WNT pathway is constitutively active in certain tissues such as colon and skin, we assessed the potential toxicity of inhibiting WNT signaling in these tissues. With 6 daily consecutive treatments of 5 mg/kg GNF-6231 intravenously (dosage and regimen used in our studies; described in Figure 2A), there was no effect on the histology of the colon (Supplementary Figure 1A), or β-catenin expression and localization as detected by immunostaining (Supplementary Figure 1B), signifying no GI tract toxicity of the drug. Likewise, no effect on skin histology (Supplementary Figure 1C) was observed in GNF-6231 treated animals compared to vehicle- treated controls.

To confirm our findings with GNF-6231 *in vitro*, we used a small molecule Casein Kinase1-alpha (CK1α) activator VU-WS113 [24], referred to in this paper as C-113. It targets the β-catenin degradation complex [24,28], and hence inhibits the WNT pathway by a mechanism of action that is distinct from GNF-6231 (Figure 1A). Quantitative real-time PCR for WNT target gene, *Axin2* showed that C-113 inhibited WNT pathway activation induced by treatment with recombinant WNT3A (Supplementary Figure 2). Since C-113 targets the WNT pathway downstream of WNT ligand secretion, it allowed us to investigate the effect of WNT inhibition without the need to overexpress *Wnt3a*.

Treatment with GNF-6231 inhibits post-MI WNT/β-catenin pathway activation in the infarcted heart and improves post-MI recovery/repair

Previous studies have shown that the canonical WNT pathway is activated in the infarcted heart starting around 72 hours post-experimental MI [4,5]. WNT pathway activation is reported to peak between 7 to 14 days post-injury, after which it begins to recede to baseline levels [5]. To avert this early, transient post-injury WNT activation, we treated mice (C57Bl6 and WNT reporter, TOPGAL mice that express β-galactosidase driven by TCF/LEF promoter [5]; age ≥ 12 weeks) with intravenous injection of 5 mg/kg GNF-6231 or vehicle (3% Vitamin E and 20% PEG 300) every 24 hours through day 6 after injury (Figure 2A). The dose and treatment regimen were determined based on our PD/PK studies and the timeline of WNT activation post-infarct described by previous studies. Immunostaining for β-catenin (in C57Bl/6J), and for β-galactosidase (in TOPGAL mice) showed that GNF-6231 treatment reduced nuclear and cytoplasmic β-catenin levels (Figures 2B and 2B′), and total β-galactosidase protein levels (Figure 2C) in the peri-infarct region compared to vehicle treatment. Furthermore, treatment with GNF-6231 reduced nuclear β-catenin activation in cardiomyocytes themselves (Supplementary Figure 3).

In order to determine the physiological effect of temporary post-MI WNT inhibition, cardiac function and remodeling were assessed at day 7 and day 30 post-MI using echocardiography

(Table 1). Heart rate was also measured by echocardiography immediately after MI (just after administration of vehicle or drug) and after 7 days and was not statistically different between drug and vehicle cohorts (data not shown). Left ventricular internal dimensions at diastole and systole (LVIDd and LVIDs respectively) were used as measures of cardiac remodeling. Day 7 measurements enable comparison between cohorts prior to any significant repair has ensued. The absence of any statistical differences among cohorts at day 7 support that the degree of MIs were not statistically different among experimental cohorts (Table 1). At day 30 post-MI, the GNF-6231 treated hearts had lower LVIDd and LVIDs compared to vehicle-treated mice (LVIDd: 3.83 ± 0.45 mm vs. 4.32 ± 0.68 mm, p=0.0377; LVIDs: 2.35 ± 0.38 mm vs. 2.84 ± 0.64 mm, p=0.0446; Table 1). To further control for variations in infarct size between mice within the experimental groups, we calculated percent change in each of the parameters from day 7 to day 30 for each individual mouse. The percent change in both of the parameters of ventricular remodeling (ΔLVIDd% and ΔLVIDs %) were significantly lower in GNF-6231 treated vs. vehicle-treated hearts (ΔLVIDd%: −2.287 ± 12.36 vs. 16.109 ± 8.53, p=0.0024; ΔLVIDs%: −3.011 ± 12.65 vs. 17.198 ± 8.91, p=0.0015; Figures 3A and 3B, Table 1), indicating that WNT inhibition prevented adverse ventricular remodeling. Ejection Fraction (EF) and Fractional Shortening (FS) are measures of cardiac function. At day 30 post-MI, GNF-6231 treated mice had higher EF (0.75 ± 0.05 vs. 0.71 ± 0.06, p=0.0421), and higher FS (38.71 ± 4.13% vs. 34.89 ± 4.86%, p=0.0325; Table 1) compared to vehicle-treated controls. The percent change from day 7 to 30 in both parameters of cardiac function (ΔEF% and ΔFS%) were on average, significantly higher for each mouse in GNF-6231 treated group compared to vehicle-treated group (ΔEF%: 0.83 ± 1.25 in GNF-6231 treated vs. −1.723 ± 2.36 in vehicle-treated, p=0.0138; and ΔFS%: 1.4 ± 2.312 in GNF-6231 treated vs. −1.713 ± 3.59 in vehicle-treated, p=0.0265; Figures 3C and 3D, Table 1), suggesting that WNT inhibition prevented worsening of cardiac function in the injured heart.

The percent infarct area, as determined by blinded histomorphometry of Masson's trichrome stained left-ventricular sections (Figures 3E and 3F) by a pathologist at day 30, was significantly lower in GNF-6231 treated hearts compared to vehicle control (9.07 ± 3.99% in GNF-6231 treated vs. 17.18 ± 4.97% in vehicle-treated; p=0.0152), indicative of a reduction in myocardial scarring with WNT inhibition. Hence, GNF-6231 augmented overall cardiac repair and recovery following LV infarct.

WNT inhibition causes proliferation of interstitial cells in the infarcted heart

Based on previous studies reporting an anti-proliferative effect of the WNT pathway in models of skeletal muscle [29] and cardiac injury [30], we asked whether the reparative effects of GNF-6231 treatment was mediated in part by proliferation of specific cardiac cells. Immunostaining for proliferation markers Ki67 and phospho-Histone-H3 (pHisH3) showed that in the peri-infarct region (defined in Figure 4A), there was a remarkable increase in $pHisH3^{+}$ cells at day 3 in both GNF-6231 and vehicle-treated hearts (Figure 4D). At day 7, the proliferative response was significantly reduced, but there were 2.3 fold more $pHisH3^{+}$ cells in the peri-infarct region of GNF-6231 treated hearts, although the difference was not statistically significant (Figure 4D). By day 15, the proliferative response had largely subsided in both treatment groups. In the distal myocardium however, GNF-6231

treated hearts had significantly more pHisH3$^+$ cells compared to vehicle-treated at both day 3 and day 7 (5.67-fold higher; ***p ≤ 0.001, and 2.65-fold higher *p ≤ 0.05 than control respectively; Figures 4B–4D).

Co-immunostaining for cardiomyocyte marker Alpha Sarcomeric Actin (αSA) with pHisH3 indicated that most of the cells that were proliferating in the distal myocardium (higher in proportion in GNF-6231 treated ventricles) were interstitial cells in both treatment and control groups (Figure 4E). This was verified by co-staining for cardiac Troponin I (cTnI) and Ki67; a representative high magnification confocal microscopy image is shown in Figure 4F. We observed rare cardiomyocytes with nuclear pHisH3 staining in both GNF-6231 treated and control animals (a representative example is shown in Figure 4G), but it wasn't clear whether these were only undergoing karyokinesis or were truly dividing cardiomyocytes. Similarly, *in vitro* BrdU (Bromodeoxyuridine) incorporation assay with HL-1 cardiomyocyte cell line showed that recombinant WNT3A and/or WNT inhibitor, C-113 had no effect on cardiomyocyte proliferation (Supplementary Figure 4C). Since the proliferating cardiomyocytes were so rare, we focused our investigations on identifying the interstitial proliferative cells.

WNT inhibition selectively reduces proliferation of myofibroblasts in the distal myocardium

In the infarcted heart, αSMA-positive myofibroblasts are the major matrix producing cells responsible for granulation tissue formation and fibrosis [16]. Hence, we performed co-immunostaining for αSMA and Ki67 (Figure 4H). Not unexpectedly, proliferating myofibroblasts (αSMA and Ki67 double positive cells) were present in both the GNF-6231 and vehicle-treated tissue, since some level of pro-fibrotic signaling is necessary to initiate granulation tissue formation and prevent infarct rupture [14]. Interestingly, in the peri-infarct region, the proportion of proliferating myofibroblasts (Ki67$^+$αSMA$^+$ cells; upper dark portions of the bar in Figure 4I) was significantly lower in the GNF-6231 treated hearts (2.21 fold lower in GNF-6231 treated; **p=0.0013) at day 3 (Figure 4I). However, the proportion of αSMA negative proliferating cells (Ki67$^+$αSMA$^-$, lower white portions of the bar in Figure 4I) in the peri-infarct region was higher in the GNF-6231 treated hearts than in vehicle-treated hearts at day 3 and day 7 post infarct (2.7-fold; p=*0.0135 and 2.2 fold; #p=0.0587 respectively; Figure 4I). Likewise, in the distal myocardium, the proportion of αSMA negative proliferating cells (Ki67$^+$αSMA$^-$ cells) was 3.3-fold higher in the GNF-6231 treated hearts than the vehicle-treated hearts at day 3 (*p=0.012) post-infarct (Supplementary Figure 5A). Meanwhile, co- immunostaining of proliferating cell nuclear antigen (PCNA) or Ki67 with markers of other fibroblast cell populations, fibroblast-specific protein-1 (FSP-1; Supplementary Figures 5B and 5C), Periostin (Supplementary Figure 5D) and Vimentin [31] (Supplementary Figure 5E) showed no effect of GNF-6231 treatment on proliferation of these cells. Based on these observations, we posit that GNF-6231 treatment selectively reduced myofibroblast proliferation in the infarcted hearts, while promoting proliferation of other interstitial cells that did not include FSP-1$^+$, Periostin$^+$ or Vimentin$^+$ fibroblasts.

WNT inhibition increases proliferation of cardiac-derived Sca1$^+$ progenitor cells

We next sought to determine the identity of the proliferating interstitial cells that were higher in number in the GNF-6231 treated hearts. To assess whether these proliferative interstitial cells were endothelial cells lining the coronary vasculature, co-immunostaining for von Willebrand factor (vWF) and PCNA was performed. Although a small percentage of proliferating endothelial cells were observed in both GNF-6231 and vehicle treated hearts, there was no significant difference in the double positive cells between the drug and vehicle treated groups (Supplementary Figures 6A and 6B).

We and others have shown that WNT inhibition causes proliferation of adult stem/progenitor cells—bone-marrow-derived MSCs [32] and cardiac tissue resident-side population progenitors [30]. Additionally, some of the proliferating interstitial cells in the immunostained sections of distal myocardium were spherical with large nuclei, and were localized in what appeared similar to ‘stem cell niche’ for tissue-resident progenitor cells described in the literature [33] (Figure 4F). These proliferative αSMA negative interstitial cells were significantly higher in proportion at the distal myocardium in GNF-6231 treated tissue compared to vehicle treated myocardium as discussed in the previous section (Supplementary Figure 5A). We hypothesized that post-injury treatment with GNF-6231 induced proliferation of a cardiac progenitor population.

We assessed the effect of WNT inhibition on Sca1$^+$CD31$^-$CD45$^-$CD117$^-$ cells isolated from murine heart homogenates by Fluorescent Activated Cell Sorting (FACS; Supplementary Figure 7A). Mice expressing thermolabile simian virus SV40 T antigen (H-2Kb-tsA58 transgenic or Immorto mice) were used for this purpose [25]. The conditionally immortalized cells isolated from these mice, under non-permissive conditions do not express the T-antigen and behave as primary cells (25). These cells were tested for multipotency based on their ability to differentiate into all three major cell types in the heart: cardiomyocytes, fibroblasts and endothelial cells (Supplementary Figures 7B and 7C).

Sca1$^+$ cells stably overexpressing *WNT3a* were generated in order to assess the proliferative response to WNT activation and subsequent inhibition with GNF-6231 or C-113. *Wnt3a* overexpression reduced proliferation compared to vector only (LZRS) control, as measured by BrdU incorporation (Figures 5A and 5B). WNT inhibition by treatment with either GNF-6231 (Figure 5A) or by C-113 (Figure 5B) for 24 hours reduced the anti-proliferative effect of *WNT3a* overexpression. Similar effects were observed in Sca1$^+$cells stably expressing *Axin2*, a WNT pathway negative regulator (data not shown). We were unable to confirm the effects WNT pathway on proliferation of Sca1$^+$ cells *in-situ* because of technical challenges in identifying *Sca1* or *c-kit* expressing progenitors in the heart by immunostaining. Interestingly, GATA4 transcription factor, which is expressed by early differentiating cardiomyocytes [34], was localized to the nucleus in more cardiomyocytes in the infarct border zone of GNF-6231 treated hearts compared to control (Figures 5C and 5D). Taken together, these observations suggest that the proliferating cells in the GNF-6231 treated myocardium may include myogenic progenitors.

WNT inhibition enhances survival of cardiomyocytes

We next asked whether the preservation of myocardial function and smaller infarct size in GNF-6231 treated animals could be accounted for, at least in part, by an effect on myocyte death or survival. Previous studies have shown that WNT inhibition by sFRP2 improves cardiomyocyte survival in the MI model [35] and in culture, specifically by binding to WNT3A and blocking its pro-apoptotic signals [36]. Terminal deoxynucleotidyl transferase (TdT) dUTP Nick-End Labeling (TUNEL) was performed to detect cell death *in situ*. Co-immunostaining for TUNEL and the cardiomyocyte marker cTnI showed that in the infarct border zone, there were significantly lower percent $TUNEL^+$ (apoptotic or necrotic) cardiomyocytes in the GNF-6231 treated hearts compared to vehicle-treated (2.03 fold lower in GNF-6231 treated ventricles; *p=0.022; Figures 6A–6C). For further verification of the positive effect of WNT inhibition on cardiomyocyte cell survival *in vitro*, cell survival and cell death assays were performed on isolated cardiomyocytes. In the mouse cardiomyocyte cell line, HL-1, cell viability was assessed by measuring metabolic activity resulting in reduction of 3-(4,5-dimethylthiazol-2-yl)-2,5-diphenyltetrazolium bromide—MTT— to insoluble formazan (MTT assay). Treatment with 50 ng/mL mouse recombinant WNT3A over 48 hours significantly reduced survival of these cells (by 16.4% over control; *$p \leq 0.05$; Figure 6D), which could be reversed by treatment with WNT inhibitor, C-113 (18.78% increase over WNT3A treatment; *$p \leq 0.05$; Figure 6D). Inhibition of WNT pathway in these cells by C-113 was determined by real-time RT-PCR for WNT target gene *Axin2* expression (Supplementary Figure 4B). Since BrdU incorporation assay had indicated no effect on proliferation of these cells by WNT pathway modulation (Supplementary Figure 4C), we concluded that the effect on cell viability was exclusively due to reduction in cell death. To further confirm these findings, we used human iPSC-derived cardiomyocytes (iCell® Cardiomyocytes[2]; Cellular Dynamics International, Madison, WI). This highly pure population of cardiomyocytes expresses cardiomyocyte markers, cTnI (Supplementary Figure 4A), and Sarcomeric Alpha Actinin (Ref [37] and manufacturer's datasheet), and beats in culture. TUNEL assay with these cells showed that in the presence of oxidative stress induced by 250 μM H_2O_2, treatment with recombinant WNT3A significantly increased cell death (percent $TUNEL^+$ cells 1.8 fold higher over control; **$p \leq 0.01$), whereas WNT inhibitor treatment reduced cell death (by 3.6 fold over WNT3A treatment; ***$p \leq 0.001$; Figures 6E and 6F), further suggesting that enhanced myocyte survival and reduced myocyte death contributed to the observed pro-reparative effect of post-injury WNT inhibition.

WNT inhibition reduces type I collagen mRNA expression by cardiac myofibroblasts

As discussed in the preceding sections, GNF-6231 treatment reduced myofibroblast proliferation compared to vehicle-treatment (Figure 4I). Since myofibroblasts are the major matrix synthesizing cells responsible for scar formation, we tested whether WNT inhibition also affected type I collagen synthesis by cardiac myofibroblasts. Primary αSMA^+ myofibroblasts (Figure 7A) were generated from adult mouse hearts as previously described [26]. Treatment of these cells with WNT inhibitor (1 μM C-113) for 48 hours reduced Collagen1α1 gene expression (by 39.16% over control; *p=0.0251) as determined by qRT-PCR (Figure 7B). These data suggest that WNT inhibition reduced pro-fibrotic effects in the

infarcted heart by modulating both the proliferation and the matrix synthesis activity of cardiac myofibroblasts.

Discussion

Several studies have reported that canonical WNT signaling is temporally increased after MI [4,5,38]. In this study we showed that temporary systemic inhibition of the WNT/β-catenin signaling by blocking WNT ligand secretion for several days post-MI prevented this post-MI tissue WNT activation. Furthermore, therapeutic WNT inhibition following infarct alleviated adverse cardiac remodeling, improved ventricular function, and reduced infarct size. These findings corroborate published reports regarding the positive effects of short term WNT inhibition with small molecule pyrvinium [11,12] on post-injury repair. While our study mirrored these reports regarding increased cell proliferation [11] and reduced cardiac myofibroblast proliferation [12] in response to WNT inhibitor treatment, we found, in contrast to these studies, that GNF-6231 did not affect endothelial cells (vWF^+) proliferation, and that increased survival of cardiomyocytes was a potential mediator of improved post-infarct recovery. These differences may be due to the limited treatment [11] and sequelae posed by toxicity of pyrvinium, blocking of both ligand-dependent and ligand-independent WNT signaling, or confounding effects of collateral inhibition of the Hedgehog signaling pathway by casein kinase1α targeted by pyrvinium [39].

Our results also differed from the study in which WNT3A/5A antagonist peptides were delivered via mini-osmotic pumps over 5 weeks following MI [10]. Although we observed similar pro-reparative effects on cardiac function, remodeling and infarct size, the effects on specific cell populations were notably different. By contrast to the increase in myofibroblast number and type I collagen synthesis, we observed a reduction in αSMA^+ myofibroblast proliferation and type I collagen expression by myofibroblasts. Given the role of myofibroblast in scar production in the heart and other organs, reduction rather than increase in myofibroblast number and activity would be expected to contribute to reduced scarring post-infarct. Effects on cardiomyocytes, progenitors and other fibroblast populations were not studied [10]. These differences in cellular effects of WNT inhibition may be attributed to incomplete targeting of the WNT pathway through a subset of WNT ligands (e.g. inhibition limited to WNT3A and WNT5A) [10], or extended treatment over the entire MI repair process.

An important strength of our study was the utilization of a therapeutically relevant small molecule, whose complete WNT inhibitory activity on all ligand-dependent WNT signals, persisted at least up to 24 hours post-intravenous injection, allowing a daily injection regimen (obviating the need to deliver biologic via mini-osmotic pump). this does not pose toxic effects on other WNT dependent tissues. Additional fine-tuning of the chemistry of the drug and dose or dosing regimen could further improve the healing outcome by Porcupine inhibition. We build on the finding that short term pharmacologic WNT inhibition improves cardiac function and reduces adverse remodeling, by an expanded investigation of the cellular mediators of this effect. Temporary WNT inhibition post-infarct increased cell proliferation and cardiomyocyte survival, and reduced myofibroblast proliferation and their matrix synthesis activity in the heart. Examination of other fibroblasts marked by expression

of FSP1 or Vimentin, and vWF^+ endothelial cells showed no effect on proliferation of these cells by GNF-6231 treatment compared to vehicle control. Whereas previous studies on pharmacologic WNT inhibition have focused on specific cellular mediators of infarct pathology (e.g.: on myofibroblast proliferation and activity, and neo-vascularization [10]), our study includes a more comprehensive examination of the cellular mediators of improved repair.

Early after infarct, WNT inhibition caused an increase in proliferation of interstitial cells, particularly in the distal myocardium. The cardiac cells that showed a proliferative response to GNF-6231 treatment mostly excluded cardiomyocytes, endothelial cells and various stromal populations, including αSMA^+ myofibroblasts, and $Vimentin^+$/$Periostin^+$/ $FSP1^+$fibroblasts. Interestingly, we discovered that WNT pathway activation downregulated proliferation of isolated $Sca1^+CD31^-CD45^-CD117^-$ cardiac progenitor cells, which are one of the tissue resident stem cells reported to reside in the interstitial niche. WNT inhibition by treatment with two mechanistically distinct WNT inhibitors, or via overexpression of *Axin2* reversed the anti- proliferative effect of WNT activation in these cells. This is in agreement with published reports of anti-proliferative effects of recombinant WNT3A on side population progenitors, *in vitro* and *in vivo* in the infarcted heart [30]. Our own work, and work by others in cardiac injury and other injury models [11,32,40] report the WNT pathway as a negative regulator of cell proliferation, particularly of stem/progenitor cells. Although these data may appear incongruous with reports of WNT being necessary for stem cell homeostasis and self-renewal in other adult organs [41–43], and during development [44,45], our data support a model in which WNT exerts multi-phasic, context dependent effects on stem cells. For example, during heart development [46], just as in skeletal muscle regeneration [29], a temporal regulation of WNT contributes to a balance between stem cell proliferation and differentiation. Also, in the now well-optimized and commercially used methods of cardiomyocyte differentiation from iPSCs, a biphasic regulation of WNT activity is sought in order to achieve optimal cardiomyocyte generation [47]. The observed expansion of $GATA4^+$ (i.e. newly differentiating) cardiomyocytes in the infarct border zone provided *in vivo* support of the role of WNT inhibition in enhancing neomyogenesis.

Our data also suggest an anti-fibrotic effect of WNT inhibition following MI. We found that WNT inhibition reduced the number of proliferating myofibroblasts *in vivo*, and also downregulated Collagen I expression in cultured cardiac myofibroblasts. These results are not surprising against the backdrop of numerous studies reporting that WNT activation is a driver of fibrosis in heart [48] and many other forms of tissue injury [49,50].

In addition to effects on cell proliferation and myofibroblast activity, WNT inhibition also reduced cardiomyocyte cell death, which is the major cause of the subsequent progression to heart failure [51]. This observation aligns with published reports of pro-apoptotic effects of WNT [30], and pro-survival effects of WNT inhibition [35,36] on cardiomyocytes.

In this study, we focused exclusively on the effects of Porcupine inhibition through the β-catenin-dependent arm of the WNT pathway based on the significant body of literature suggesting a critical and complicated role—both maladaptive [6,7,30], and in some cases pro-reparative [13,14,16]—for this signaling cascade in infarct pathology. However, since

GNF-6231 targets Porcupine, its effects independent of canonical WNT pathway may also be important. Porcupine acyltransferase activity is specifically targeted towards WNT ligands [20,22], and hence other pathways are unlikely to be affected. However, Porcupine inhibition can also affect the non-canonical arms of the WNT pathway.

There are reports implicating both the Ca^{2+}/CAM Kinase and the JNK arms of the non-canonical WNT signaling pathways [34,52] in infarct pathology and repair. Hence, future studies investigating the effect of inhibition of WNT ligand secretion on the non-canonical arms of the WNT signaling pathways may provide a more complete picture of the mechanisms mediating cardiac recovery by Porcupine inhibitor treatment. Moreover, WNT/β-catenin pathway can be activated downstream of ligand binding through cross-talks with other pathways such as TGFβ [53,54]. The contribution of ligand-independent WNT pathway activation in infarct pathology remains unclear. Development of a biocompatible agonist of the WNT/β-catenin degradation complex (similar to pyrvinium, but without the toxicity) would be useful in answering these questions.

That said, our data demonstrating the potential of short term WNT inhibition in counteracting the key drivers of post-infarct LV dysfunction and eventual failure—cardiomyocyte death and fibrosis—are clinically significant since the current standard-of-care for myocardial infarct focus mainly on thrombolytic and palliative interventions, and do not address the ongoing disease progression driven by the initial infarct. Moreover, in the context of complicated [5,9,13,16,32] and multifaceted roles of the WNT pathway in infarct repair in the existing literature, our data may speak to the potential of temporally regulated scalable pharmacologic WNT inhibition in reconciling the discordant observations based on genetic models [6,7,14] of WNT modulation. With additional details on the mechanism-of-action and safety data emerging with continuing studies, and ongoing clinical trials [23], GNF-6231 and the new class of Porcupine inhibitors hold significant potential as effective therapeutics for cardiac regeneration.

Supplementary Material

Refer to Web version on PubMed Central for supplementary material.

Acknowledgments

We would like to acknowledge Dr. Antonis K. Hatzopoulos for providing the TOPGAL mice, Dr. Ethan Lee for C-113, the Genomics Institute of Novartis Research Foundation for GNF-6231, the Translational Pathology Shared Resource (TPSR) at Vanderbilt University Medical Center for aid in specimen preparation for histology, and Dr. Bin Li and Dr. Caressa Lietman for their constructive criticism.

Funding

This work was supported by the Veterans Affairs Merit Award, NIH grants R21EB019509-01A1, and 1R01GM118300 to PPY, and Vanderbilt University Clinical and Translational Science Award [Grant number UL1 RR024975-01] from National Center for Research Resources (NCRR)/National Institute of Health (NIH), and philanthropic funds to PPY; and the American Heart Association Predoctoral Fellowship [3PRE16080004] to DB.

References

1. Mozaffarian D, Benjamin EJ, Go AS, Arnett DK, Blaha MJ, et al. Heart disease and stroke statistics–2015 update: a report from the American Heart Association. Circulation. 2015; 131:e29–e322. [PubMed: 25520374]
2. Mill JG, Stefanon I, dos Santos L, Baldo MP. Remodeling in the ischemic heart: the stepwise progression for heart failure. Braz J Med Biol Res. 2011; 44:890–898. [PubMed: 21829898]
3. Sutton MG, Sharpe N. Left ventricular remodeling after myocardial infarction: pathophysiology and therapy. Circ. 2000; 101:2981–2988.
4. Oerlemans MI, Goumans MJ, van Middelaar B, Clevers H, Doevendans PA, et al. Active WNT signaling in response to cardiac injury. Basic Res Cardiol. 2010; 105:631–641. [PubMed: 20373104]
5. Aisagbonhi O, Rai M, Ryzhov S, Atria N, Feoktistov I, et al. Experimental myocardial infarction triggers canonical WNT signaling and endothelial-to-mesenchymal transition. Dis Model Mech. 2011; 4:469–483. [PubMed: 21324930]
6. Zelarayan LC, Noack C, Sekkali B, Kmecova J, Gehrke C, et al. Beta-Catenin downregulation attenuates ischemic cardiac remodeling through enhanced resident precursor cell differentiation. Proc Natl Acad Sci USA. 2008; 105:19762–19767. [PubMed: 19073933]
7. Baurand A, Zelarayan L, Betney R, Gehrke C, Dunger S, et al. Beta-catenin downregulation is required for adaptive cardiac remodeling. Circ Res. 2007; 100:1353–1362. [PubMed: 17413044]
8. Barandon L, Couffinhal T, Ezan J, Dufourcq P, Costet P, et al. Reduction of infarct size and prevention of cardiac rupture in transgenic mice overexpressing FrzA. Circ. 2003; 108:2282–2289.
9. He W, Zhang L, Ni A, Zhang Z, Mirotsou M, et al. Exogenously administered secreted frizzled related protein 2 (Sfrp2) reduces fibrosis and improves cardiac function in a rat model of myocardial infarction. Proc Natl Acad Sci U S A. 2010; 107:21110–21115. [PubMed: 21078975]
10. Laeremans H, Hackeng TM, van Zandvoort MA, Thijssen VL, Janssen BJ, et al. Blocking of frizzled signaling with a homologous peptide fragment of WNT3a/WNT5a reduces infarct expansion and prevents the development of heart failure after myocardial infarction. Circ. 2011; 124:1626–1635.
11. Saraswati S, Alfaro MP, Thorne CA, Atkinson J, Lee E, et al. Pyrvinium, a potent small molecule WNT inhibitor, promotes wound repair and post-MI cardiac remodeling. PLoS One. 2010; 5:e15521. [PubMed: 21170416]
12. Murakoshi M, Saiki K, Urayama K, Sato TN. An anthelmintic drug, pyrvinium pamoate, thwarts fibrosis and ameliorates myocardial contractile dysfunction in a mouse model of myocardial infarction. PLoS One. 2013; 8:e79374. [PubMed: 24223934]
13. Paik DT, Rai M, Ryzhov S, Sanders LN, Aisagbonhi O, et al. WNT10b Gain-of- Function Improves Cardiac Repair by Arteriole Formation and Attenuation of Fibrosis. Circ Res. 2015; 117:804–816. [PubMed: 26338900]
14. Duan J, Gherghe C, Liu D, Hamlett E, Srikantha L, et al. WNT1/β catenin injury response activates the epicardium and cardiac fibroblasts to promote cardiac repair. EMBO J. 2012; 31:429–442. [PubMed: 22085926]
15. Woulfe KC, Gao E, Lal H, Harris D, Fan Q, et al. Glycogen synthase kinase- 3beta regulates post-myocardial infarction remodeling and stress-induced cardiomyocyte proliferation *in vivo*. Circ Res. 2010; 106:1635–1645. [PubMed: 20360256]
16. Hahn JY, Cho HJ, Bae JW, Yuk HS, Kim KI, et al. Beta-catenin overexpression reduces myocardial infarct size through differential effects on cardiomyocytes and cardiac fibroblasts. J Biol Chem. 2006; 281:30979–30989. [PubMed: 16920707]
17. von Gise A, Zhou B, Honor LB, Ma Q, Petryk A, et al. WT1 regulates epicardial epithelial to mesenchymal transition through beta-catenin and retinoic acid signaling pathways. Dev Biol. 2011; 356:421–431. [PubMed: 21663736]
18. Anastas JN, Moon RT. WNT signalling pathways as therapeutic targets in cancer. Nat Rev Cancer. 2013; 13:11–26. [PubMed: 23258168]
19. Kahn M. Can we safely target the WNT pathway? Nat Rev Drug Discov. 2014; 13:513–532. [PubMed: 24981364]

20. Nusse R. WNTs and Hedgehogs: lipid-modified proteins and similarities in signaling mechanisms at the cell surface. Development. 2003; 130:5297–5305. [PubMed: 14530294]
21. Liu J, Pan S, Hsieh MH, Ng N, Sun F, et al. Targeting WNT-driven cancer through the inhibition of Porcupine by LGK974. Proc Natl Acad Sci U S A. 2013; 110:20224–20229. [PubMed: 24277854]
22. Herr P, Hausmann G, Basler K. WNT secretion and signalling in human disease. Trends Mol Med. 2012; 18:483–493. [PubMed: 22796206]
23. Novartis P. A Study of Oral LGK974 in Patients with Malignancies Dependent on WNT Ligands. 2014
24. Thorne CA, Hanson AJ, Schneider J, Tahinci E, Orton D, et al. Small-molecule inhibition of WNT signaling through activation of casein kinase 1alpha. Nat Chem Biol. 2010; 6:829–836. [PubMed: 20890287]
25. Ryzhov S, Goldstein AE, Novitskiy SV, Blackburn MR, Biaggioni I, et al. Role of A2B adenosine receptors in regulation of paracrine functions of stem cell antigen 1-positive cardiac stromal cells. J Pharmacol Exp Ther. 2012; 341:764–774. [PubMed: 22431204]
26. Kong P, Christia P, Saxena A, Su Y, Frangogiannis NG. Lack of specificity of fibroblast-specific protein 1 in cardiac remodeling and fibrosis. Am J Physiol Heart Circ Physiol. 2013; 305:H1363–H1372. [PubMed: 23997102]
27. Cheng D, Liu J, Han D, Zhang G, Hsieh M, et al. Discovery of a Novel Series of Pyridinyl Acetamide Derivatives as Potent, Selective, and Orally Bioavailable Porcupine Inhibitors. 2016
28. Bastakoty D, Saraswati S, Cates J, Lee E, Nanney LB, et al. Inhibition of WNT/beta-catenin pathway promotes regenerative repair of cutaneous and cartilage injury. FASEB J. 2015; 29:4881–4892. [PubMed: 26268926]
29. Brack AS, Conboy IM, Conboy MJ, Shen JR, Rando TA. A temporal switch from notch to WNT signaling in muscle stem cells is necessary for normal adult myogenesis. Cell Stem Cell. 2008; 2:50–69. [PubMed: 18371421]
30. Oikonomopoulos A, Sereti KI, Conyers F, Bauer M, Liao A, et al. WNT signaling exerts an antiproliferative effect on adult cardiac progenitor cells through IGFBP3. Circ Res. 2011; 109:1363–1374. [PubMed: 22034491]
31. Zeisberg EM, Kalluri R. Origins of cardiac fibroblasts. Circ Res. 2010; 107:1304–1312. [PubMed: 21106947]
32. Alfaro MP, Pagni M, Vincent A, Atkinson J, Hill MF, et al. A WNT modulator sFRP2 enhances mesenchymal stem cell engraftment, granulation tissue formation and myocardial repair. Proc Natl Acad Sci USA. 2008; 105:18366–18371. [PubMed: 19017790]
33. Kimura W, Sadek HA. The cardiac hypoxic niche: emerging role of hypoxic microenvironment in cardiac progenitors. Cardiovasc Diagn Ther. 2012; 2:278–289. [PubMed: 24282728]
34. Schmeckpeper J, Verma A, Yin L, Beigi F, Zhang L, et al. Inhibition of WNT6 by Sfrp2 regulates adult cardiac progenitor cell differentiation by differential modulation of WNT pathways. J Mol Cell Cardiol. 2015; 85:215–225. [PubMed: 26071893]
35. Mirotsou M, Zhang Z, Deb A, Zhang L, Gnecchi M, et al. Secreted frizzled related protein 2 (sFRP2) is the key Akt-mesenchymal stem cell-released paracrine factor mediating myocardial survival and repair. Proc Natl Acad Sci USA. 2007; 104:1643–1648. [PubMed: 17251350]
36. Zhang Z, Deb A, Pachori A, He W, Guo J, et al. Secreted frizzled related protein 2 protects cells from apoptosis by blocking the effect of canonical WNT3a. J Mol Cell Cardiol. 2009; 46:370–377. [PubMed: 19109969]
37. Zhang J, Wilson GF, Soerens AG, Koonce CH, Yu J, et al. Functional cardiomyocytes derived from human induced pluripotent stem cells. Circ Res. 2009; 104:e30–e41. [PubMed: 19213953]
38. Blankesteijn WM, Essers-Janssen YP, Verluyten MJ, Daemen MJ, Smits JF. A homologue of Drosophila tissue polarity gene frizzled is expressed in migrating myofibroblasts in the infarcted rat heart. Nat Med. 1997; 3:541–544. [PubMed: 9142123]
39. Li B, Fei DL, Flaveny CA, Dahmane N, Baubet V, et al. Pyrvinium attenuates Hedgehog signaling downstream of smoothened. Cancer Res. 2014; 74:4811–4821. [PubMed: 24994715]
40. Brack AS, Conboy MJ, Roy S, Lee M, Kuo CJ, et al. Increased WNT signaling during aging alters muscle stem cell fate and increased fibrosis. Science. 2007; 317:807–810. [PubMed: 17690295]

41. Fevr T, Robine S, Louvard D, Huelsken J. WNT/beta-catenin is essential for intestinal homeostasis and maintenance of intestinal stem cells. Mol Cell Biol. 2007; 27:7551–7559. [PubMed: 17785439]
42. Huelsken J, Vogel R, Erdmann B, Cotsarelis G, Birchmeier W. β-Catenin controls hair follicle morphogenesis and stem cell differentiation in the skin. Cell. 2001; 105:533–545. [PubMed: 11371349]
43. Plaks V, Brenot A, Lawson DA, Linnemann JR, Van Kappel EC, et al. Lgr5-expressing cells are sufficient and necessary for postnatal mammary gland organogenesis. Cell Rep. 2013; 3:70–78. [PubMed: 23352663]
44. Merrill BJ. WNT pathway regulation of embryonic stem cell self-renewal. Cold Spring Harb Perspect Biol. 2012; 4:a007971. [PubMed: 22952393]
45. Kelly KF, Ng DY, Jayakumaran G, Wood GA, Koide H, et al. β-catenin enhances Oct-4 activity and reinforces pluripotency through a TCF-independent mechanism. Cell Stem Cell. 2011; 8:214–227. [PubMed: 21295277]
46. Hurlstone AF, Haramis AP, Wienholds E, Begthel H, Korving J, et al. The WNT/β-catenin pathway regulates cardiac valve formation. Nature. 2003; 425:633–637. [PubMed: 14534590]
47. Lian X, Hsiao C, Wilson G, Zhu K, Hazeltine LB, et al. Robust cardiomyocyte differentiation from human pluripotent stem cells via temporal modulation of canonical WNT signaling. Proc Natl Acad Sci U S A. 2012; 109:E1848–E1857. [PubMed: 22645348]
48. Bergmann MW. WNT signaling in adult cardiac hypertrophy and remodeling: lessons learned from cardiac development. Circ Res. 2010; 107:1198–1208. [PubMed: 21071717]
49. Akhmetshina A, Palumbo K, Dees C, Bergmann C, Venalis P, et al. Activation of canonical WNT signalling is required for TGF-beta-mediated fibrosis. Nat Commun. 2012; 3:735. [PubMed: 22415826]
50. He W, Dai C, Li Y, Zeng G, Monga SP, et al. WNT/β-catenin signaling promotes renal interstitial fibrosis. J Am Soc Nephrol. 2009; 20:765–776. [PubMed: 19297557]
51. Ruiz-Meana M, Garcia-Dorado D. Translational cardiovascular medicine (II). Pathophysiology of ischemia-reperfusion injury: new therapeutic options for acute myocardial infarction. Rev Esp Cardiol. 2009; 62:199–209. [PubMed: 19232193]
52. Wang Y, Su B, Sah VP, Brown JH, Han J, et al. Cardiac hypertrophy induced by mitogen-activated protein kinase kinase 7, a specific activator for c-Jun NH2-terminal kinase in ventricular muscle cells. J Biol Chem. 1998; 273:5423–5426. [PubMed: 9488659]
53. Labbe E, Lock L, Letamendia A, Gorska AE, Gryfe R, et al. Transcriptional cooperation between the transforming growth factor-beta and WNT pathways in mammary and intestinal tumorigenesis. Cancer Res. 2007; 67:75–84. [PubMed: 17210685]
54. Hu MC, Rosenblum ND. Smad1, β-catenin and Tcf4 associate in a molecular complex with the Myc promoter in dysplastic renal tissue and cooperate to control Myc transcription. Development. 2005; 132:215–125. [PubMed: 15576399]

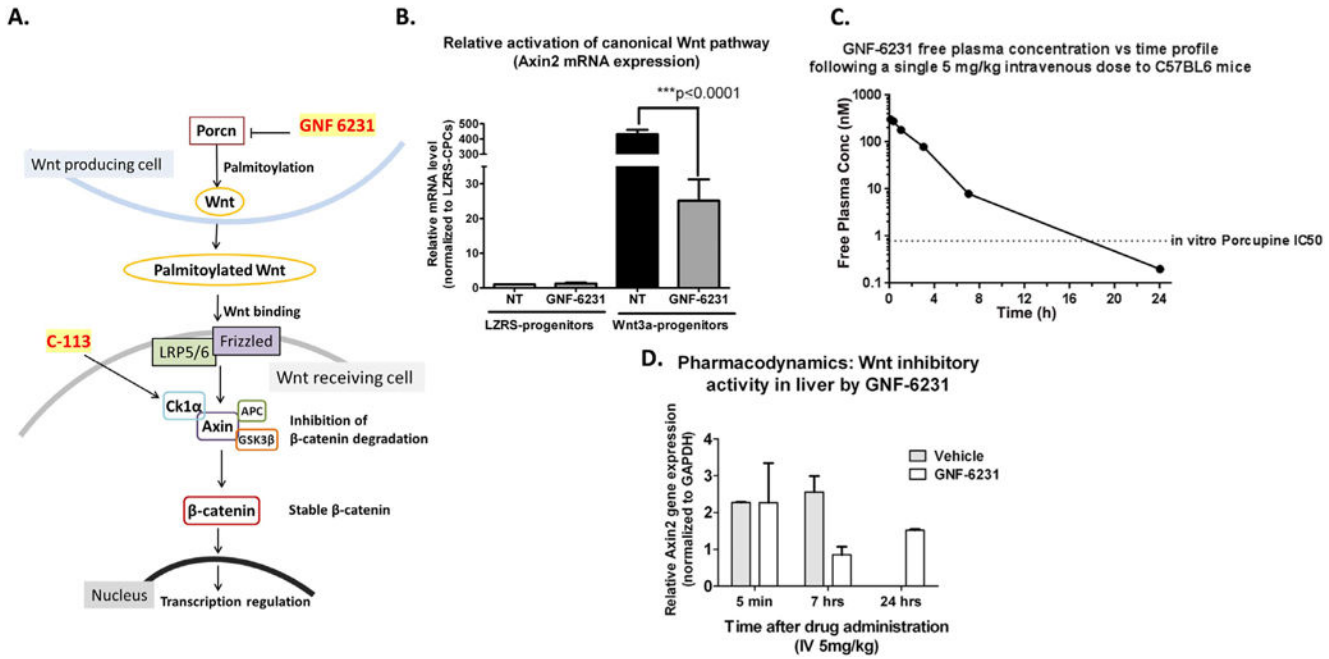

Figure 1. GNF-6231 inhibits canonical WNT pathway activity *in vitro*

(A) Schematic of the WNT pathway and point of action of WNT inhibitors, GNF-6231 and C-113. **(B)** Fold change in *Axin2* gene expression in *WNT3a* overexpressing cardiac cells showing GNF-6231 treatment reduced WNT target gene expression (*N=3* replicates from independent experiments; ***$p \leq 0.0001$; Repeated measures ANOVA with Bonferroni correction for multiple comparisons). **(C)** IV free plasma level of GNF-6231 after a single intravenous injection of 5 mg/kg. The plasma half-life of the drug was approximately 2.3 hours; GNF-6231 free plasma concentrations were above the *in vitro* Porcupine IC50 for >12 h. **(D)** qRT-PCR showed inhibition of *Axin2* gene expression in liver at different time points following a single 5 mg/kg intravenous treatment with GNF-6231 (*N=2* mice per timepoint). Bars represent Mean ± SD.

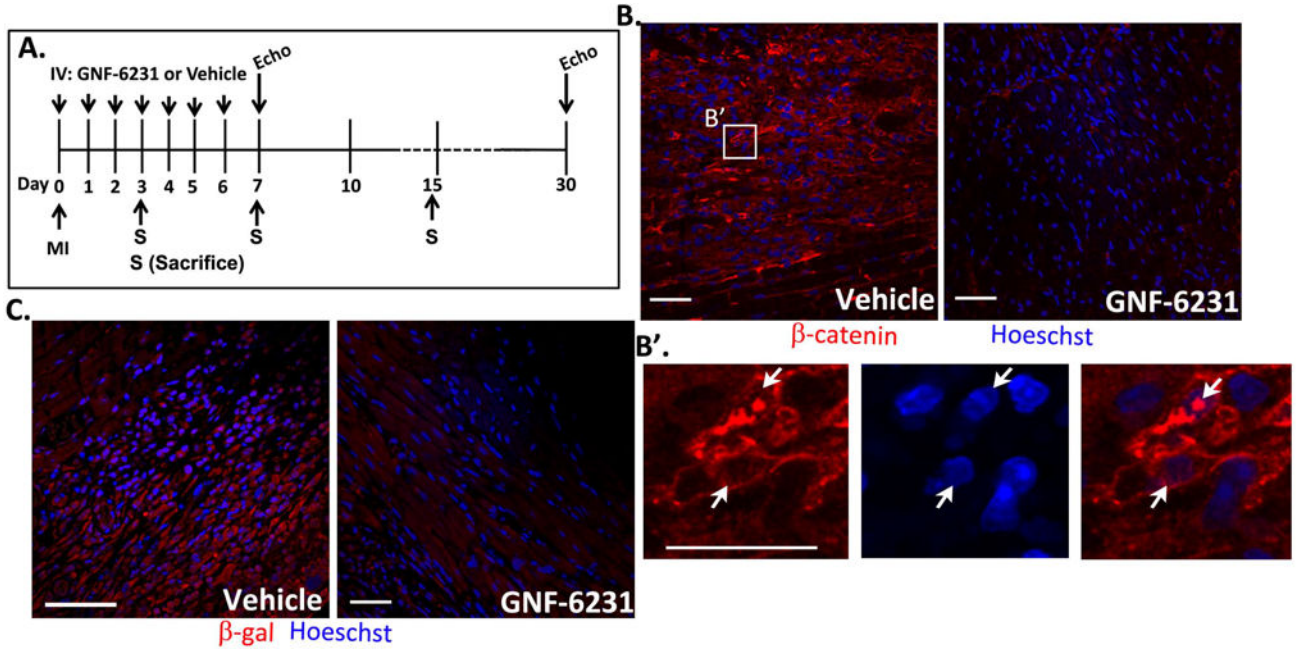

Figure 2. Porcupine inhibitor treatment inhibits WNT pathway activity in the infarcted heart

(A) Schematic summarizing animal study timelines. Mice were treated with daily intravenous injection of 5 mg/kg drug or vehicle following MI and continued through day 6. For cardiac recovery studies, mice underwent echocardiography at days 7 and 30. For histology, a separate cohort of mice was sacrificed on days 3, 7 and 15. **(B)** β-catenin immunostaining of peri- infarct region of ventricles at day 7 showed reduction in β-catenin levels with GNF-6231 treatment. **(B′)** High magnification image of vehicle-treated tissue showed nuclear localization of β-catenin signifying WNT pathway activation. **(C)** β-galactosidase immunostaining in ventricle sections from WNT reporter, TOPGAL mice demonstrated inhibition in WNT activity at day 7 post-infarct with GNF-6231 treatment. Scale bars equal 50 μm. Images are representative of sections from $N \geq 3$ mice; at least 4 areas were imaged from each mouse.

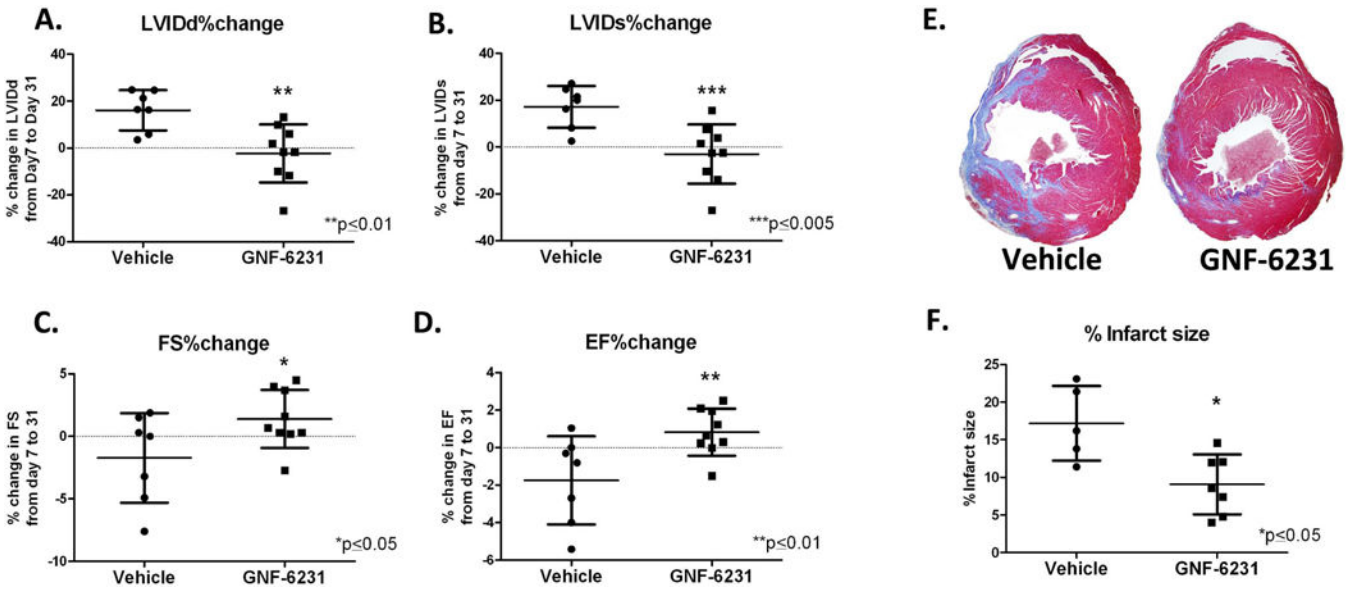

Figure 3. Porcupine inhibition improves cardiac function and reduces adverse remodeling after MI

Left ventricular remodeling was measured as % change in **(A)** LVIDd and **(B)** LVIDs. LV function was measured as % change in **(C)** FS and **(D)** EF. Data showed no increase in left ventricular diameter (A and B), and improved cardiac function (C and D) with GNF-6231 treatment compared to vehicle. **(E)** Masson's trichrome stained representative sections of the left ventricle at day 30 depicted more collagen stained (blue) area in vehicle-treated LV compared to GNF-6231-treated. **(F)** Quantification of infarct size. Each data point on graphs represents individual mouse; *$*p \leq 0.05$, $**p \leq 0.01$ or $***p \leq 0.005$*; unpaired t-test.

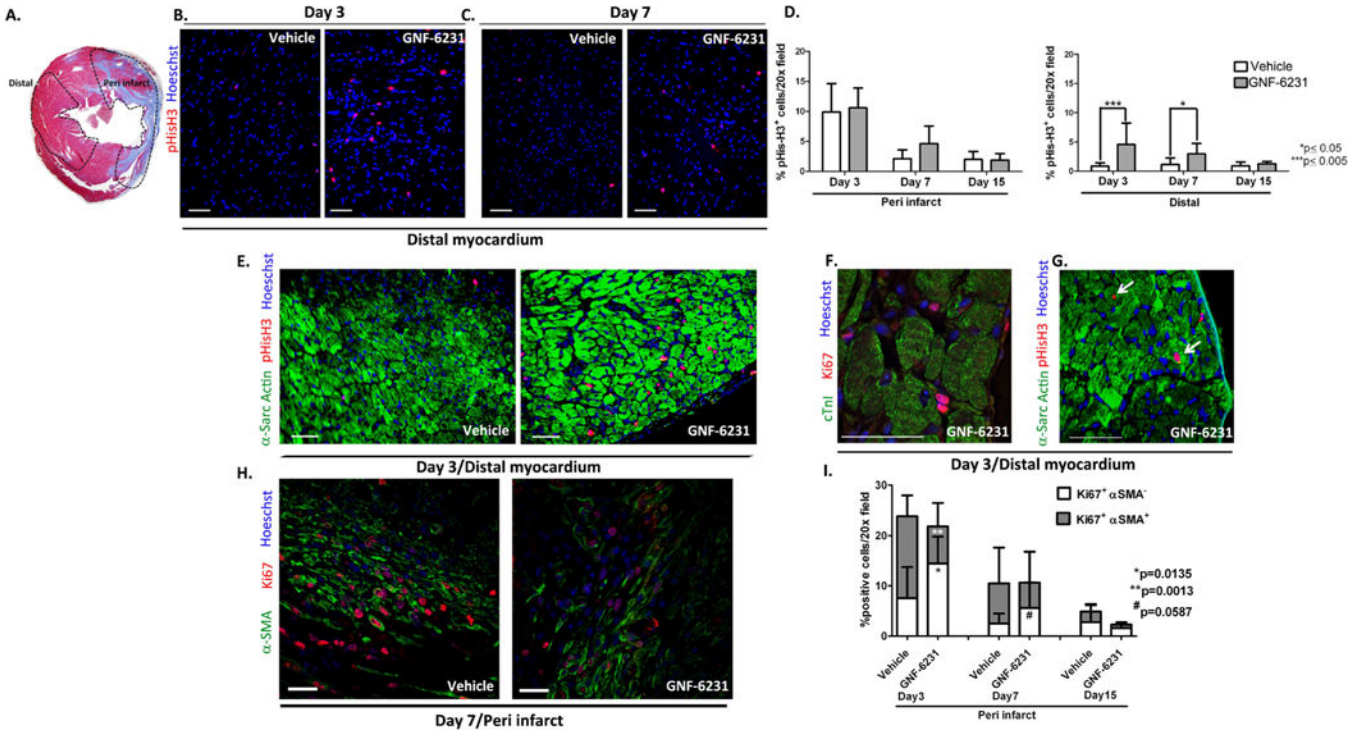

Figure 4. WNT inhibition promotes proliferation of interstitial αSMA negative cells in the infarcted heart

(A) H&E stained cross-section of the heart demarcating peri-infarct and distal regions of the left ventricle as defined in the study. Representative pHisH3 stained sections of the ventricles at **(B)** day 3 and **(C)** day 7 showing more proliferative cells in the distal myocardium of GNF-6231 treated hearts. **(D)** Quantification of percent pHisH3^{+} cells. Bars represent mean ± SD; $N \geq 4$ images of sections from $N \geq 3$ mice per group were imaged; $*p \leq 0.05$, $***p \leq 0.005$; One-Way ANOVA with Bonferroni Correction for multiple comparisons. Representative sections of the distal myocardium at day 3 post-MI **(E)** co-stained with αSarcomeric Actin and pHisH3, and **(F)** high magnification confocal microscopy image of ventricle co-stained with cTnI and Ki67, demonstrating that the majority of proliferative cells in the GNF-6231-treated tissue localized to the interstitium of myofibers. **(G)** αSarcomeric Actin/pHisH3 co-stained LV depicting the rare proliferating cardiomyocytes (white arrows). **(H)** Proliferating myofibroblasts were identified by αSMA/Ki67 co-staining as depicted in the representative section from the peri-infarct region at day 7. **(I)** Quantification of αSMA/Ki67 co-stained cells revealed that the percentage of proliferating myofibroblasts (grey shaded portion of the bars) was significantly lower in GNF-6231-treated peri-infarct tissue than control at day 3 ($**p=0.0013$) and lower ($^{\#}p=0.0587$) at day 7. In contrast, the percentage of proliferating non-myofibroblasts (αSMA^{-} cells; lower white portion of the graphs) was significantly higher ($*p=0.0135$) in GNF-6231 treated ventricles compared to control at day 7. Bars represent mean ± SD. $N \geq 12$: at least 3 separate sections from at least 3 mice per group were imaged. *P-values* for individual comparisons between each two groups of data were calculated using Mann-Whitney test. Scale bars equal 50 μm.

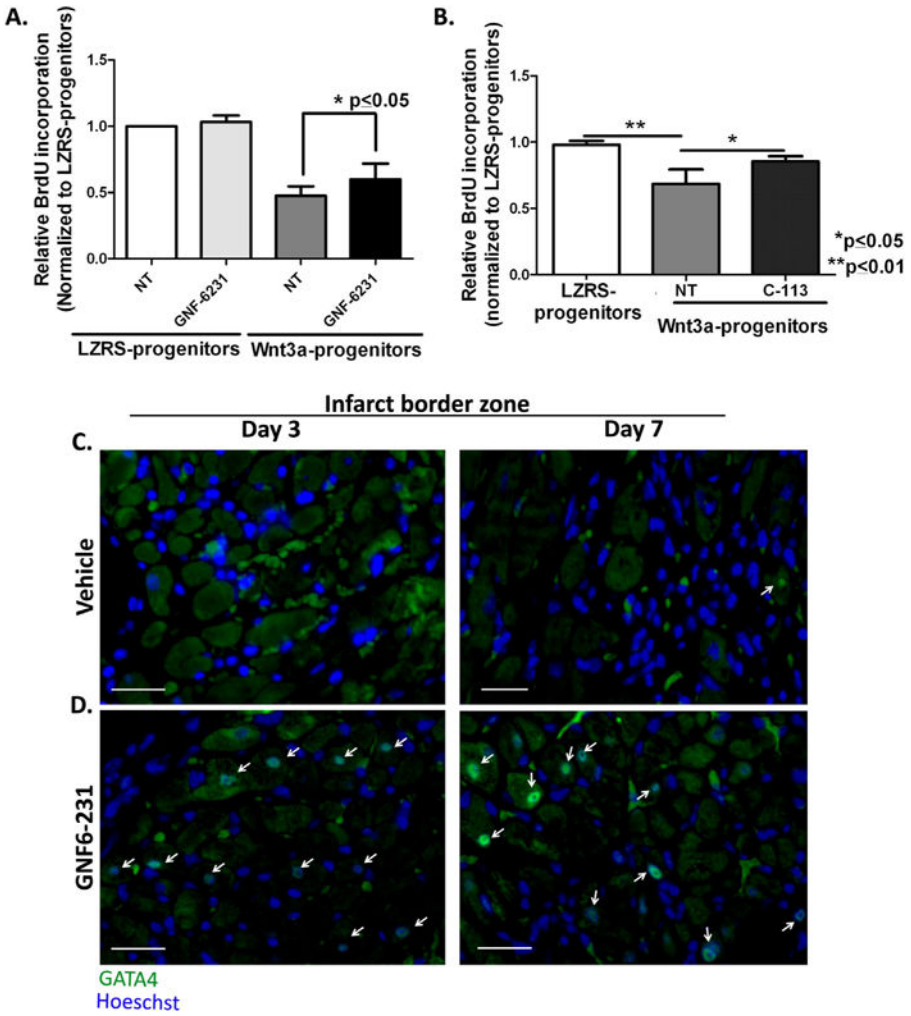

Figure 5. WNT inhibition increases proliferation of progenitor cells that may contribute to myogenesis

(A and B) Relative BrdU incorporation by $Sca1^{+}$ progenitor cells stably expressing LZRS (empty vector) or *Wnt3a*-LZRS revealed that proliferation was reduced by *Wnt3a* overexpression and this effect was reversed by (A) GNF-6231 treatment and (B) C-113 treatment.

Data are presented as Mean ± SD. (A) $N=5$ and (B) $N=3$ replicates from independent experiments; $*p \leq 0.05$ and $**p \leq 0.01$; Kruskal-Wallis test with Dunns correction for multiple comparisons. **(C and D)** Representative GATA4 immunostained sections of infarct border zone at day 3 (left panels) and day 7 (right panels) post-MI of (C) vehicle-treated hearts and (D) GNF-6231 treated hearts. White arrows point to GATA4 stained nuclei. Scale bars equal 50 μm; the images are representative of at least 4 sections each from $N \geq 3$ mice per group.

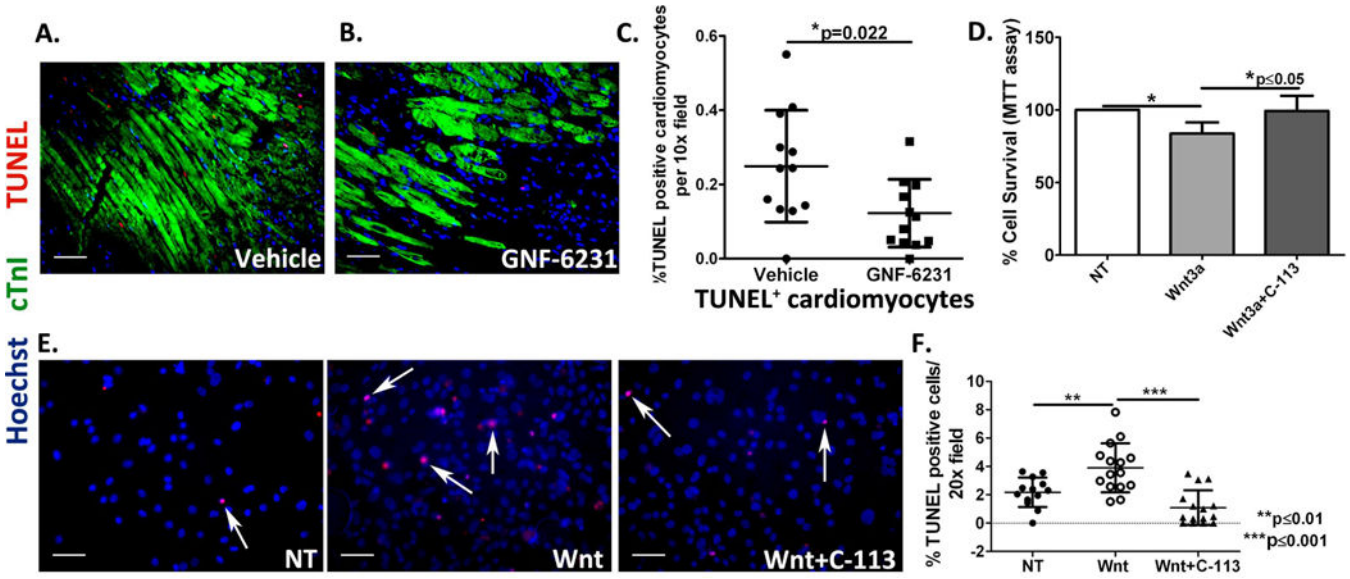

Figure 6. WNT inhibition reduces cardiomyocyte cell death

(A and B) Representative sections co-stained with cTnI and TUNEL of infarct border zone of (A) vehicle-treated hearts, and (B) GNF-6231 treated hearts. **(C)** Quantification of percent TUNEL positive cardiomyocytes revealed significantly fewer apoptotic cardiomyocytes in GNF-6231 treated hearts. *N=5* mice per group, at least 4 sections imaged per mouse, **p=0.022*, unpaired t-test. **(D)** Percent cell survival of HL-1 rat cardiomyocytes as measured by metabolic uptake (MTT) assay showed significant reduction in survival with recombinant WNT3A treatment, which was rescued by addition of C-113. Bars represent mean ± SD; *N=3* replicates from independent experiments; **P ≤ 0.05;* Kruskal- Wallis test with Dunns correction for multiple comparisons. **(E)** Representative images of human iPSC-derived iCell cardiomyocytes treated with recombinant WNT3A or WNT3A and C-113 in presence of 250 μM H_2O_2 showing that under stress, treatment with recombinant WNT3A increased cell death, which was rescued by WNT inhibition with C-113. **(F)** Quantification of %TUNEL positive iCell cardiomyocytes per 20× field. *N ≥ 12* per group, at least 4 areas imaged in each replicate from 3 independently run experiments; ***p ≤ 0.01* and ****p ≤ 0.001*; One-Way ANOVA with Bonferroni correction for multiple comparisons. Scale bars in A-B and E represent 50 μm.

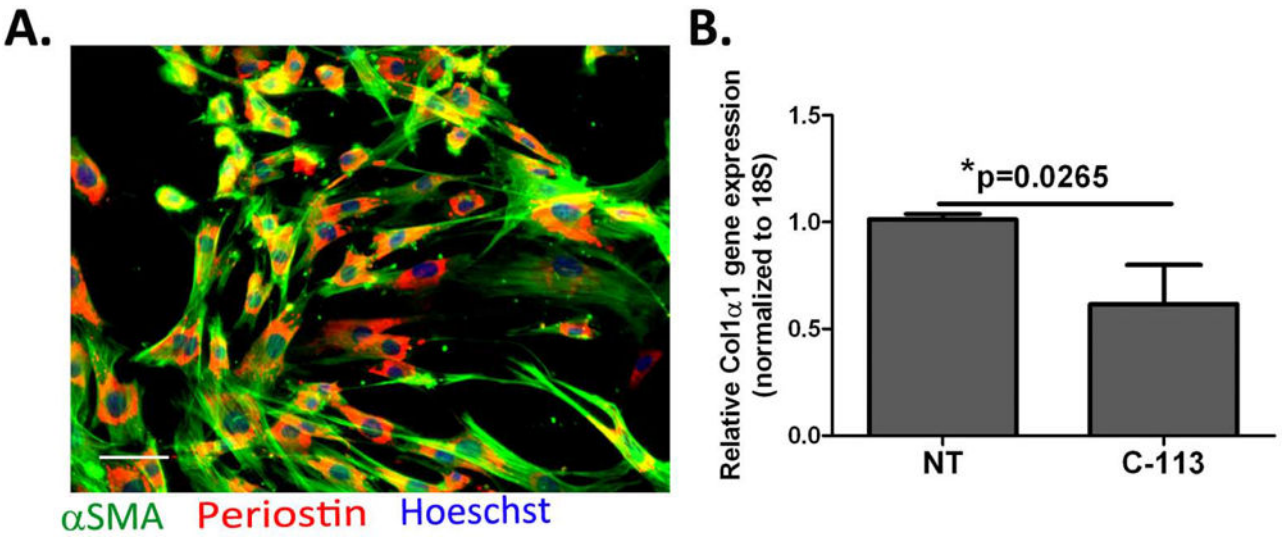

Figure 7. WNT inhibition reduces collagen synthesis activity *in vitro*

(A) Primary myofibroblasts in culture confirmed by αSMA (green) and Periostin (red) staining; scale bar equals 50 μm. **(B)** Relative *Col1α1* gene expression in primary cardiac myofibroblasts with and without WNT inhibitor treatement revealed significant reduction in *Col1α1* gene expression in response to WNT inhibitor treatment. Bars represent mean ± SD. *N=4* replicates from independent experiments; **p=0.0265*; Mann-Whitney test.

Table 1

GNF-6231 treatment improves cardiac recovery post-MI The top eight rows represent mean ± SD values for each parameter and treatment at day 7 and 30. The mean ± SD percent difference between day 7 and day 30 for each mouse (Δ) are listed in the bottom four rows. Statistical difference between parameters in each two columns was determined by unpaired t-test.

Echo parameters		Vehicle	GNF-6231	p-values
LVIDd (mm)	Day 7	3.74 ± 0.60	3.95 ± 0.42	ns; p=0.3229
	Day 30	4.32 ± 0.68	3.83 ± 0.45	*p=0.0377
LVIDs (mm)	Day 7	2.43 ± 0.55	2.45 ± 0.39	ns; p=0.7378
	Day 30	2.84 ± 0.64	2.35 ± 0.38	*p=0.0446
FS%	Day 7	35.48 ± 4.65	38.24 ± 4.69	ns; p=0.174
	Day 30	34.89 ± 4.86	38.71 ± 4.13	*p=0.0325
EF	Day 7	0.72 ± 0.06	0.75 ± 0.06	ns; p=0.149
	Day 30	0.71 ± 0.06	0.75 ± 0.05	*p=0.0421
Δ LVIDd%		16.109 ± 8.53	−2.287 ± 12.36	**p=0.0024
Δ LVIDs%		17.198 ± 8.91	−3.011 ± 12.65	**p=0.0015
Δ FS%		−1.713 ± 3.59	1.4 ± 2.312	*p=0.0265
Δ EF%		−1.723 ± 2.36	0.83 ± 1.25	**p=0.0138
N		7	9	